Highly Cross-Linked Epoxy Resins: An Atomistic Molecular Dynamics Simulation Combined with a Mapping/Reverse Mapping Procedure

Pavel V. Komarov,*,†,‡ Chiu Yu-Tsung,† Chen Shih-Ming,† Pavel G. Khalatur,§,|| and Peter Reineker○

Material and Chemical Research Laboratory of Industrial Technology Research Institute, Chutung, Hsinchu 31040, Taiwan, Department of Theoretical Physics, Tver State University, Tver 170002, Russia, Institute of Organoelement Compounds, Russian Academy of Science, Moscow 119991, Russia, Department of Polymer Science, University of Ulm, Ulm D-89069, Germany, and Department of Theoretical Physics, University of Ulm, Ulm D-89069, Germany

Received March 22, 2007; Revised Manuscript Received August 4, 2007

ABSTRACT: This paper presents a new computational method for simulating polymer network formation. There are four separate procedures involved in the methodology for this multiscale simulation: (i) mapping of the polymerizing monomers onto a coarse-grained model, (ii) cross-linking the monomers by applying Monte Carlo simulation to the coarse-grained model, (iii) reverse mapping of the coarse-grained model to a fully atomistic representation, and (iv) simulation of the atomistic model through standard molecular dynamics technique. Molecular dynamics simulations and experimental studies are carried out to check the algorithm on the basis of the determination of the physical properties of the cycloaliphatic epoxy resin which is prepared from 3,4-epoxycyclohexylmethyl-3,4-epoxycyclohexanecarboxylate as resin monomers and 4-methylhexahydrophthalic anhydride as curing agents. Depending on the effective conversion and temperature, we determine the density, the glass transition temperature, and the thermal expansion coefficient of the cross-linked epoxy system. An increase in the degree of cross-linking is found to increase the glass transition temperature. Good agreement between computer simulation and experimental results is achieved for highly cross-linked networks, thereby showing that the simulation model is basically valid.

1. Introduction

The fabrication of new materials with high functional performance is an important aim of modern industrial progress. A promising way in this direction is the optimization of the internal structure of rubberlike materials by embedding nanoparticles. Nanocomposites that are based on polymer networks with inorganic fillers have attracted great attention due to their versatility and the unique properties of their microstructure.[1−8] The performance and strength of many nanocomposites, hybrid and thin multilayered material systems are very much dependent upon the structural and mechanical properties of network matrices. Theoretical studies in this direction face a serious challenge because there is no conventional way to build atomistic models of specific polymers, which form a network. To construct such models, one should take into account such factors as the chemical structure, the sizes, the degree of branching of macromolecules, the number of cross-links between them, etc.

Most of the classical network theories rely on single chain models.[9−14] These theories replace the true molecular network by an idealized network of identical Gaussian chains, each of which consists of freely jointed links whose orientation is completely independent of the positions of all others. The behavior of the entire network system is then supposed to be given by the partition function of the single chain raised to the power of the number of chains. Cross-linked networks constructed from chains of this nature do not exhibit changes in internal energy with deformation at constant volume and temperature, and thus deviate from the results of experimental stress-temperature measurements. Deviations from Gaussian behavior as a consequence of finite chain extensibility also present certain difficulties which cannot be overcome by the use of "equivalent" freely jointed chains.[15−17] The existing theories of non-Gaussian chains[18−21] are inadequate on this account. Another drawback of these single chain type theories is that they ignore the effect of quenched disorder stemming from the cross-links and the intrinsic irregularity of the topological structure of networks, which originates in the randomness of the irreversible cross-linking process. Also, experimental studies have drawn attention to other limitations of the classical network theories: while the results of mechanical measurements are reasonably described by Flory−Rehner-type theories which are based on the hypothesis of affine network deformation,[21] small-angle neutron scattering (SANS) experiments show that this approach is violated on micro- and mesoscopic scales.[22−28] This behavior mainly stems from the fact that highly cross-linked polymer networks exhibit typical solid-like elastic response on macroscopic scales, while on microscopic nanometer scales there are liquid-like fluctuations which are similar to those observed in solutions of non-cross-linked macromolecules.[29] Experimentally, the liquid-like component is subtracted by assuming that this component is the same as that from the corresponding polymer solution and by using a theoretical scattering intensity function for semidilute polymer solutions.[23−28] The static frozen-inhomogeneities in-

* To whom correspondence should be addressed. E-mail: kpv@germany.ru.
† Material and Chemical Research Laboratory of Industrial Technology Research Institute.
‡ Department of Theoretical Physics, Tver State University.
§ Institute of Organoelement Compounds, Russian Academy of Science.
|| Department of Polymer Science, University of Ulm.
○ Department of Theoretical Physics, University of Ulm.

10.1021/ma070702+ CCC: $37.00 © 2007 American Chemical Society
Published on Web 10/02/2007

troduced by topological constraint at network preparation are strongly influenced by the preparation conditions and the degree of cross-linking. Thus, the highly cross-linked polymer networks have both solid-like and liquid-like properties.

Network deformation, such as swelling in a solvent or uniaxial extension, can be readily performed in the laboratory. From such experiments, macroscopic properties such as equilibrium swelling ratios, elastic moduli, and stress−strain behavior can be determined. These macroscopic properties, however, depend strongly on the microscopic structure of the network. Microscopic properties, including the distribution of cross-links and their density, cannot be determined as easily using experiments. The partial structure factors and radial distribution functions are the only structural quantities which can experimentally be measured with high accuracy and which provide information on atomic distribution and order in the system. However, these measurements do not give any data about the number of cross-links between monomers, the degree of cross-linking/branching of the polymer chains, etc. Also, it should be noted that the static scattering itself is unable to decompose the dynamic and static components of the scattered intensity because it provides only information about the ensemble average of the spatial inhomogeneity of the sample.[23−28]

Because presently there is no comprehensive understanding of the interrelation between the microscopic properties of polymer networks and the conditions of their synthesis, as always, under these circumstances, an alternative to physical experiments and analytical theories is computer simulations, which are designed to obtain a numerical answer without knowledge of an analytical solution. In this paper, our attention will be focused on the atomistic model of highly cross-linked epoxy resins. Naturally, the model should reflect the specific structural properties of the macromolecules from which the network is composed.

There are some characteristics of polymer networks that make them difficult to simulate. Real rubberlike materials relax slowly relative to time scales accessible by molecular simulations. One of the major causes of this sluggishness is their cross-link constraint. In fact, the slow relaxation times of networks have prevented continuous, dynamical simulations of deformation. Another difficulty is related to the atomistic simulation of irreversible cross-linking process.

Computational techniques for modeling polymer networks have emerged rapidly in recent years as an important complement to experiment. Many papers have been published which have applied computer simulation to the formation of polymer networks and to the calculation of their structural properties (see, e.g., refs 30−59). However, practically none of these studies are of a fully atomistic type.

During the past decade, several groups have reported methods for building atomistic polymer networks. Using an atomistic model and molecular simulation techniques, Hamerton et al. have carried out the study of two network polycyanurates based on the dicyanates of bisphenol A and an oligomeric poly(ary1ene ether sulfone).[60−62] For this system, elastic moduli and glass transition temperatures were predicted in reasonable agreement with the experimental values. Doherty et al. have developed the so-called polymerization molecular dynamics to build poly(methacrylate) networks.[63] Yarovsky and Evans have simulated various model stages of the hydrolysis reaction during the sol/gel processing in the systems of organofunctionalized silanes and an organic polymer in aqueous solution.[64] Recently, the structure and elastic moduli of end-cross-linked poly(dimethylsiloxane) networks have been studied by Heine and co-workers using molecular dynamics at the united atom level.[65]

The present work is aimed at developing a new methodology for the construction of atomistic models of highly cross-linked polymer networks with application of this methodology to epoxy resins with different cross-link density. Epoxy resins are a class of thermoset materials used extensively in structural and specialty composite applications because they offer a unique combination of properties that are unattainable with other thermoset resins.[66−68] Available in a wide variety of physical forms from low-viscosity liquid to high-melting solids, they are amenable to a wide range of processes and applications. The epoxy resins possess high glass transition temperatures (190−260 °C), show low dielectric loss behavior and low moisture absorption, are tough, and show good peel strength. In their range of applications as high performance materials the glass transition temperature T_g of the cured resins is extremely important as it largely governs the use temperature. Hence, an ability to predict this parameter would be of major importance in designing new materials, including epoxy-based nanocomposites.

The cross-linking and toughening process of epoxy resins was first simulated by Alperstein et al.,[69] using a commercial polymer modeling software package NETWORK.[70] Very recently, Wu and Xu have developed a method to construct atomistic molecular models of cross-linked polymers.[71] The calculations were carried out for an industrially important amine-cured epoxy resin based on diglycidyl ether of bisphenol A (DGEBA) with isophorone diamine as a cross-linker. A polymer network with conversion up to 93.7% was generated using the commercial molecular simulation package Cerius^2 from Accelrys.[72] Density and elastic constants of the system were calculated from the equilibrated structure for the validation of the generated models. Yarovsky and Evans proposed a more complex polymer network model for low-molecular-weight water-soluble epoxy resins cross-linked with different curing agents (tributoxymethyl melamine and tetramethylol glycoluril).[73] The polymer network was formed dynamically during molecular dynamics simulations based on the software from Accelrys.[72] Our approach described in this paper has a similarity in spirit to these methods but is somewhat different. In particular, it provides flexible control over the details of the network formation process in a much simpler way than through the use of closed commercial molecular simulation packages. Also, in the published articles,[69,71,73] the calculations based on the commercial packages were available only for relatively small system sizes (a little larger than 10^3 atoms). In this work, we report results for significantly larger scale models.

Particularly for polymers of complex architecture, it can be difficult to produce bulk structures at realistic densities. Often hybrid methods are adopted, since for example, straightforward energy minimization leads to structures trapped in local minima whereas molecular dynamics is difficult to carry out over a long enough time to allow relaxation of polymer motion. To correctly capture the physics of macromolecules over a full range of relevant length and time scales, multiscale modeling techniques have been devised.[74−83] These attempts to map the molecular structure and long-range motion onto a simplified model. Especially interesting are methods that allow a relaxed bulk structure to be reverse-mapped back to a realistic model with atomistic detail. In this paper, we employ this strategy to simulate the formation of highly cross-linked epoxy networks and their structural and thermophysical properties.

The rest of the paper is organized as follows: in section 2, we describe experimental methods used for synthesis and

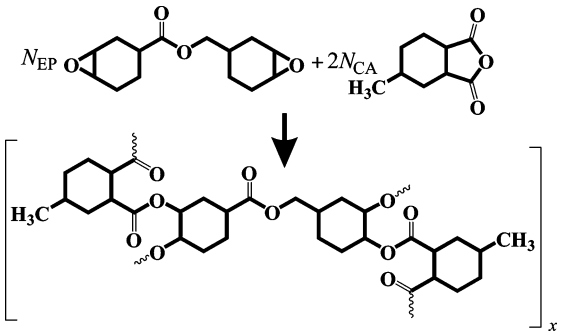

Figure 1. 3,4-Epoxycyclohexylmethyl−3,4−epoxycyclohexanecarboxylate (epoxy monomer, EP) and 4-methylhexahydrophthalic anhydride (curing agent, CA) and a cross-linked network fragment.

characterization of the cycloaliphatic epoxy resins; the model and computational methods are explained in section 3; the results are given in the next section; and the conclusions are given in section 5.

2. Experimental Part

The main goal of our experimental study is to obtain the properties of the cycloaliphatic epoxy resin, CAER, as an example of polymer network for comparisons with the simulation results. CAER was selected because it is an important engineering matrix material for polymeric composites where a high glass transition temperature is wanted. Different properties and curing conditions of a number of resins have been well studied.[84] For our purposes, CAER was obtained from a set of two polymerizing monomers: 3,4-epoxycyclohexylmethyl-3,4-epoxycyclohexanecarboxylate as epoxy monomers, EP (supplied by Union Carbide), and 4-methylhexahydrophthalic anhydride, MHHPA (supplied by Alusuisse, Italia), as curing agents, CA. All the materials were used as received. The formation of epoxy network, which contains N_{EP} EP monomers and N_{CA} CA monomers, can be depicted by the scheme shown in Figure 1.

To prepare the samples, the epoxy resin was mixed with anhydride and catalyst. The catalyst used for the synthesis was benzyldimethylamine, BDMA, in a ratio of 1:100 of the total mass of the sample. In order to remove small bubbles, the resulting compound was degassed under vacuum in an oven. After that, it was slowly cast into a mold to avoid bubble creation. Then, the mold was put into the vacuum oven to ensure that there are no bubbles trapped in the bulk of the mixture. The specimens were cured at 170 °C for 1 h and then cooled down to room temperature.

An optimum mass ratio of EP/CA was chosen under the condition to obtain the epoxy resin with the maximum glass transition temperature, T_g. This is achieved when a polymer network has the largest cross-linking density. Accurate determination of the ratio of epoxy to curing agent is important because a variation of more than ±2% of the stoichiometric ratio of epoxy to curing agent can have a significant effect on the final properties of the cured resin. After several experiments, we chose the proportion 10:19 as the optimum ratio.

It should be noted that during the chemical reaction, a certain amount of epoxide homopolymerization occurs in competition with the formation of polyester linkages and leads to a polyether structure. The cross-links of the molecular network are provided by the tetrafunctional epoxide. The mole ratios of epoxide and 4-methylhexahydrophthalic anhydride used in the synthesis reflect the relative amounts of the competing reactions.

The glass transition temperature and the thermal expansion coefficient of the cured materials were measured using a thermal mechanical analyzer (model Q400, TA Instruments Inc.). The sample was tested with 5 °C/min scanning rate from room temperature up to 250 °C. The density of the samples was measured before curing at ambient temperature by directly measuring the sample using a pycnometer. For the cured samples, the density was determined indirectly by the flotation method.

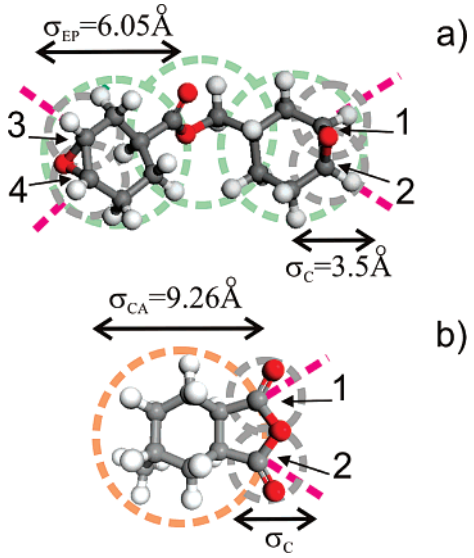

Figure 2. Minimum energy structures of (a) EP and (b) CA monomers and their schematic coarse-grained representation (dashed circles). Numbers indicate "reactive sites".

The following physical properties were obtained: the density $\rho = 1.175 \pm 0.005$ g/cm^3, the glass transition temperature $T_g = 440.5 \pm 2.5$ K, and the volume thermal expansion coefficient $\beta = 0.000195 \pm 0.000015$ K^{-1}. The values of ρ and β were measured at room temperature.

3. Model and Simulation Methodology

There are four separate procedures involved in the methodology for our multiscale simulation: (i) mapping of the polymerizing monomers onto a coarse-grained model, (ii) cross-linking the monomers by applying Monte Carlo (MC) simulation to the coarse-grained model, (iii) reverse mapping of the coarse-grained model to a fully atomistic representation, and (iv) simulation of the atomistic model through standard molecular dynamics (MD) technique.

We might expect the results of the atomistic simulations of epoxy resins to be sensitive to the details of the potential models, where a reasonably delicate balance between steric and packing effects and electrostatic types of interactions should be present. Hence it is important that the choice of model should be made carefully. For example, an all-atom model should contain all the various internal modes of motion. Obviously a balanced set of charges on atoms is very important in quantitative describing the structural and thermophysical properties of CAER.

For the EP and CA monomers as well as for different oligomers arising as a result of the reaction between EP and CA, the calculations of the structural parameters and atomic partial charges were performed at the *ab initio* unrestricted UHF/6-31G** and UMP2/6-31G** levels. Fully optimized molecular geometries were found by using the Polak-Ribiere conjugate gradient method. For charge distribution analysis, we used a Mulliken charge distribution calculated at the UMP2/6-31G** level. The minimal energy structures found for the EP and CA monomers are shown in Figure 2.

3.1. Sample Preparation. Step 1: Network Building Procedure. The reaction mechanism between an anhydride curing agent and epoxy resin is complex, because, as mentioned above, competing reactions take place. The anhydride reacts with the epoxy hydroxyls to form half-esters. The half-ester containing the free carboxyl group is then available to react with an epoxide ring, which generates another hydroxyl. The newly formed hydroxyl can react with another anhydride or it can react with another epoxy to form an ether linkage.

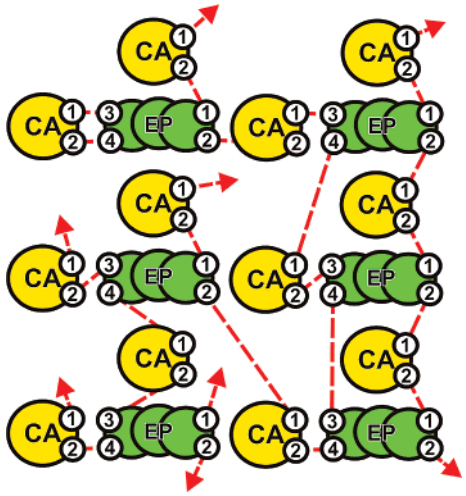

Figure 3. Logical schema illustrating the coding of cross-links in an epoxy polymer network. Numbers indicate "reactive sites".

Although chemical reactions cannot be treated implicitly in MD simulations and the simulations are run for relatively short times, they have two major advantages compared with experiments: They can be performed on model systems with simple interparticle interactions, for which detailed theoretical calculations can be carried out. And, they give access to many physical properties, e.g., to correlation functions, which would be difficult to obtain experimentally. One of the aims of our calculation is to construct a chemically reasonable network topology with a high percent conversion comparable to experiment.

The structure of the monomers EP and CA was coarse grained. To this end, they were represented by 7-site and 3-site rigid bodies, respectively, as shown in Figure 2. In particular, each EP monomer was modeled by three fused spheres of diameter $\sigma_{EP} = 6.05$ Å arranged in a nearly linear fashion and by four spheres of diameter $\sigma_C = 3.5$ Å that correspond to the terminal "reactive sites" of epoxy rings and are centered at the positions of carbon atoms 1, 2, 3, and 4 (Figure 2a). Each CA monomer was represented by a sphere of diameter $\sigma_{CA} = 9.26$ Å with two attached "reactive sites" of size σ_C which are centered at the positions of carbon atoms 1 and 2 of 5-membered ring (Figure 2b). The parameters σ_{EP}, σ_{CA}, and σ_C were estimated from the geometries and molar volumes of the corresponding molecules. The sites of type σ_C constitute the potential cross-link "reactive sites". They are numbered from 1 to 4 (for EP) and from 1 to 2 (for CA), as shown in Figure 2. Note that the diameter σ_C defines the cross-link distance between two connected monomers in our coarse-grained network model.

The cross-link "reactive sites" of the coarse-grained monomers (CGM) were encoded by a square matrix $||\Delta_{\alpha\beta}||$; $\alpha, \beta = 1, 2, ..., m$, where m is the total number of the "reactive sites" in the system. For the elements of this topology matrix, we assume that $\Delta_{\alpha\beta} = 1$ if sites α and β are connected and $\Delta_{\alpha\beta} = 0$ otherwise. Figure 3 depicts schematically the topology of a fully cross-linked coarse-grained network.

In our network building procedure, the centers-of-masses of N_{EP} and N_{CA} coarse-grained monomers were placed randomly on a simple cubic lattice. No catalyst molecules were simulated. The assumptions incorporated into the model are that the structure of the CGMs is fixed, and that free CGMs may diffuse rotationally and translationally. The system size of the monomer mixture was determined by satisfying the following two criteria: (i) the monomer ratio N_{EP}:N_{CA} should correspond to an experimental stoichiometric ratio and (ii) the density of the uncross-linked mixture should be close to the experimental density. When placed on the lattice, CGMs were placed in random rotational orientations. Initially, m elements ($m = 4N_{EP} + 2N_{CA}$) of the topology matrix $||\Delta_{\alpha\beta}||$ were set to zero. The system density was $\rho = 1$ g/cm^3. Then, using a random number generator, N_{link} cross-links were generated randomly between free "reactive sites". A reaction radius R_{link} ranging from 4 to 9 Å was employed. This makes the model nonlocal in that CGMs can interact over some spatial and angular ranges. When two "reactive sites" α and β are closer than R_{link}, a "chemical reaction" takes place, and a covalent bond $\alpha-\beta$ is formed. The usual periodic boundary conditions were employed. In order to join the central simulation cell to the imaginary cells, we used the method described by Weber and Helfand[85] and, in more detail, by Doherty et al.[63] The reaction propagates by a constantly growing capture radius R_{link}. The total number of cross-links N_{link} is viewed as a parameter in our calculation. It was assumed that 90% of cross-links can be created between epoxy monomers and curing agents and 10% of cross-links can connect epoxy monomers. This ratio corresponds to our experimental results as well to the available literature data.[86] All the information about the monomer connections was stored in the $||\Delta_{\alpha\beta}||$ matrix.

Step 2: System Refinement and Relaxation. As monomers are cross-linked together in the network building process, the resulting structures may also be assumed highly extended, forming branched structures and too long bonds. Therefore, the system should be relaxed and checked for unnatural bond lengths possibly formed during the network building process. To this end, MC simulations were performed in the *NVT* ensemble by using the classical Metropolis sampling procedure.[87]

We assume that all the sites of CGMs interact via a repulsive excluded volume potential

$$V_{ev}(r_{ij}) = \begin{cases} 4\epsilon_{ij}\left[\left(\frac{\sigma_i+\sigma_j}{2r_{ij}}\right)^{12} - \left(\frac{\sigma_i+\sigma_j}{2r_{ij}}\right)^{6} + \frac{1}{4}\right] & \forall \; r_{ij} \le \frac{\sigma_i+\sigma_j}{2} \\ 0 & \forall \; r_{ij} > \frac{\sigma_i+\sigma_j}{2} \end{cases} \quad (1)$$

where r_{ij} is the distance between interacting sites i and j ($i, j = 1, 2, ..., 7N_{EP} + 3N_{CA}$) and ϵ_{ij} is the energy parameter. Another contribution to the energy of the coarse-grained system is related to the deformation of cross-links. This contribution is described by the following harmonic potential

$$V_{link}^{(\alpha\beta)} = \frac{1}{2}\kappa_{\alpha\beta}\left(|\mathbf{r}_{\alpha\beta}| - \frac{\sigma_\alpha + \sigma_\beta}{2}\right)^2 \quad (2)$$

where $\kappa_{\alpha\beta}$ is the energy parameter and $|\mathbf{r}_{\alpha\beta}|$ is the distance between "reactive sites" α and β. The total energy of the coarse-grained system is given by

$$V_{CGS} = \sum_{i>j=1}^{7N_{EP}+3N_{CA}} V_{ev}(r_{ij}) + \sum_{\substack{\alpha,\beta=1 \\ \alpha\neq\beta}}^{m=4N_{EP}+2N_{CA}} \Delta_{\alpha\beta} V_{link}^{(\alpha\beta)} \quad (3)$$

In eq 1, we set $\epsilon_{ij} = 1$ (in units of k_BT). To ensure a "strong chemical bond" acting over a short range, the value $\kappa_{\alpha\beta} = 2 \times 10^3\ k_BT$Å^{-2} was used in the subsequent coarse-grained simulations. It should be noted that the value of $\kappa_{\alpha\beta}$ is rather arbitrary and can be varied to control the rate of monomer assembly.

In the MC simulations, two different equiprobable types of displacements in continuum space for CGMs were used, viz., translation and rotation. The transition probability from an old configuration **O** to a new one **N** is P(**O**→**N**) = min {1, exp-

$(\Delta V_{CGS}/k_BT)\}$, where ΔV_{CGS} is the difference between the old and new total system energy (3) and $k_BT = 1$. Depending on the system density and a predefined number of cross-links N_{link}, from 10^6 to 10^7 MC steps are needed in order to relax the model system, where one MC step is defined as an average of one MC trial move on all particles comprising the system. It should be stressed that the main goal of this calculation is to assemble the coarse-grained monomers and to remove local mechanical stresses that are due to cross-link bonds of length greater than σ_C, which can arise from the generation of cross-links based on distance criteria R_{link} between predefined "reactive sites". Thus, the final system energy does not necessarily correspond to the global energy minimum and optimal network configuration. During the MC relaxation procedure, the coarse-grained polymer network is checked for too long cross-links. If such bonds are present, they are removed. On the other hand, if the conversion ratio is lower than the prescribed number of cross-links N_{link}, additional bonds are added to obtain more complete cross-linking conversion. We assume that, once a new bond has been formed, it cannot be broken if it is close to σ_C. Newly formed cross-links confine the relaxation of the system. When a new bond forms, the nonbonded interaction (1) between the two corresponding CGM sites is turned off. If a given bond is removed, the nonbonded interaction between the corresponding sites is switched on. In this case, we set $\Delta_{\alpha\beta} = 0$ in eq 3. If it is necessary, the MC relaxation is repeated again. As a result, we obtain the final topology matrix $||\Delta_{\alpha\beta}||$ and coordinates of the CGM sites.

To account for the statistical distribution of the simulation results related to the random cross-link topology, each calculation should be repeated many times. Because of the naturally slow relaxation of the highly cross-linked system, however, we were only able to make a limited number of runs. In this study, the network building procedure and the subsequent MC relaxation were repeated several times starting from different initial configurations, and the results reported below are the averages over five independent runs carried out for each conversion.

Step 3: Reverse Mapping. For a current relaxed and refined network structure obtained for the coarse-grained Monte Carlo model, we carried out a reverse mapping procedure. To this end, the missing carbon and oxygen atoms were first inserted into the confined space occupied by each CGM, taking into account correct bond lengths and bond angles. Then all of the hydrogen atoms were attached to the carbon atoms. Because the positions of coarse-grained sites were defined in terms of the atom positions of the atomistic model, the reverse mapping is relatively straightforward. Generally, our reverse mapping procedure was similar to that described in detail in many recent publications.[74−83] Having the coordinates of CGM sites, the atomic coordinates can be easily restored. Local stresses and close contacts between different atoms as well as too long chemical bonds connecting different monomers and corresponding bond angles are left to relax out by standard atomistic molecular dynamics simulations.

In these simulations, the short *NVT* runs were performed with the bending, torsion, and electrostatic interactions switched on, while the LJ potential was introduced very gradually (MD simulations are described below in more detail). At this initial stage, velocities were rescaled at each time step to compensate for the large amount of heat produced in the system. In these simulation runs, the total and potential energies showed an initial decrease, possibly with a few separate stages, and then fluctuated around a constant value, indicating the achievement of the equilibrium state. The resulting network is chemically reasonable in terms of bond lengths and bond angles.

It should be noted that during constant temperature simulations, the system expanded to release the internal stress. Usually, its density is lower as compared to the real epoxy resin. Therefore, it needs to be further optimized.

3.2. Step 4: MD Simulation. The structural and physical properties of the model epoxy resins with different numbers of monomers and cross-links obtained as described above were studied by molecular dynamics simulations. In the constant pressure (*NPT*) MD simulations, it is straightforward to construct the OPLS/AA model for the CAER system based on the work by Jorgensen and co-workers.[88−91] The total potential energy of the system was represented as a sum of the bond stretching, bond-angle bending and dihedral torsion energies as well as the van der Waals (Lennard-Jones, LJ) and electrostatic (Coulomb) terms, $V = V_b + V_\Theta + V_\varphi + V_{vdw} + V_e$. Both short-ranged van der Waals and long-ranged electrostatic interactions between all atoms were explicitly included in the model. LJ parameters for the cross interactions were obtained using the standard Lorentz−Berthelot combining rules. The electrostatic interactions were computed using the Ewald summation technique.[92] The values of the largest reciprocal space vector ("reciprocal space cutoff", q_{max}) and the Ewald convergence parameter, α, were preliminary determined in order to obtain an accuracy of 10^{-6} in the Coulombic energy and varied between different system sizes. Values for q_{max} ranged from 8 to 9, while values of α ranged from 0.34 to 0.36 Å^{-1} (typical values are $\alpha = 0.345$ Å^{-1} and $q_{max} = 8.8$). With these parameters for the Ewald sum, the difference between the direct and indirect calculations of the reciprocal space contribution to the pressure was found to be less than 0.2 atm. The dielectric constant ϵ was assumed to be 1, since all partial charges were treated explicitly.

All the systems were simulated under *NPT* conditions. The temperature and pressure were maintained by the Nose-Hoover thermostat[93] using the modular-invariant method.[94] The pressure P was maintained at the required value by loose coupling with a τ_P of 800 fs. The corresponding Nose relaxation time, τ_T, was set to 30 fs. The equations of motion were integrated using the reversible double time step algorithm r-RESPA[92,95] in which all forces were divided into two groups, "fast" and "slow". The first group is determined by covalent bonds, bond angles, and dihedral angles; it also includes LJ forces and real-space electrostatic forces within a short cutoff distance, R_s, of 5 Å. The second group includes LJ and real-space electrostatic forces in the range between R_s and a "long" cutoff distance R_c as well as reciprocal-space electrostatic interactions.

Periodic boundary conditions were assumed in order to model the bulk system, and for computational efficiency, a cutoff was applied to nonbond interactions between atoms separated by more than 10 Å. (To avoid potential discontinuities, the pair potential was smoothly raised to zero over 0.5 Å.) The 10 Å cutoff was chosen to be smaller than half the edge of the simulation cell in order to avoid interactions between an atom and its "image" due to the periodic boundary conditions. Long-range corrections to the energy and pressure are made.[96] An atomic Verlet neighbor list was used, which was updated every 15 time steps; neighbors were included if they were closer than 11 Å. The equations of motion were solved using a leapfrog version of the Verlet−Störmer algorithm[97] with "fast" time step, Δt_f, of 0.4 fs and "slow" time step, $\Delta t_s = 10\Delta t_f$.

In the equilibration runs, the cross-linked structures obtained as described in section 3.1 were first gradually compressed (at

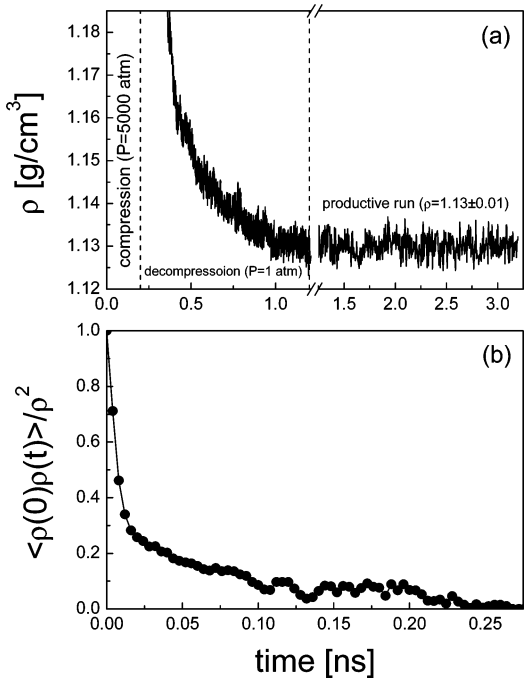

Figure 4. (a) Density as a function of simulation time for a polymer network constructed from $N_{EP} = 64$ EP monomers and $N_{CA} = 128$ EA monomers connected by 230 cross-links. (b) Normalized time autocorrelation function $\langle\rho(0)\rho(t)\rangle/\rho^2$ calculated for the same system during productive MD run.

$P = 5000$ atm) and then the pressure was gradually reduced to $P = 1$ atm over a period of 200 ps. Each compression−decompression cycle was repeated three times. The calculations were then continued during 1 ns of MD run at $P = 1$ atm until an equilibrium system density was reached. The productive MD simulations at $P = 1$ atm were run for 2.0 ns. For each percent conversion, five independently generated systems were simulated.

Figure 4a shows the typical time dependence of the system density for a polymer network constructed from $N_{EP} = 64$ EP monomers and $N_{CA} = 128$ EA monomers connected by 230 cross-links. In Figure 4b, we show the normalized time autocorrelation function $\langle\rho(0)\rho(t)\rangle/\rho^2$ calculated for the same system during productive MD run. Both results indicate that the simulation is long enough to achieve thermodynamic equilibrium. The rate with which $\langle\rho(0)\rho(t)\rangle/\rho^2$ drops to zero is a measure of how fast the system forgets the long-range conformational characteristics of its initial configuration and, therefore, provides a measure of the effectiveness of the simulation method in equilibrating the system. It is observed from Figure 4b that the $\langle\rho(0)\rho(t)\rangle/\rho^2$ drops to zero after about 0.25 ns.

In the course of the productive runs carried out for the equilibrated systems, configurations were saved at intervals of 100 fs and used subsequently to calculate structural properties. The steady-state temperature was varied from 250 to 650 K. The final structure from each simulation was used as the starting structure for the next simulation at lower temperature.

4. Results and Discussion

The simulated bicomponent epoxy systems usually contained $N_{EP} = 64$ and $N_{CA} = 128$ monomers. The chosen ratio $N_{EP}/N_{CA} = 0.5$ approximately corresponds to the optimal mass ratio found in our experimental study (Sec. 2). The system as a whole involved about 5000 atoms (192 cross-linked monomers). Note that the total number of atoms depends on the number of cross-links, N_{link}, present in the system. For this system, the value of N_{link} was changed from 0 to the maximal achievable calculated conversion (≈90%) when $N_{link}^{(max)} \approx 230$ (practically fully cross-linked network). A typical snapshot of the cross-linked structure is shown in Figure 5. Generally, the final percent conversion, C, in our simulations ranged from 0 to 94%, the latter value is comparable to experimental epoxy resins. In should be noted that a full 100% conversion cannot be obtained experimentally because of glass transition at later stage of synthesis.

Local Structure. The local structure of the simulated system was examined by the pair correlation functions (PCF), $g(r)$. Figure 6 shows the partial PCFs $g_{CC}(r)$ calculated for carbon atoms at different C. In the range $r < 4$ Å, several well-pronounced peaks are observed. They characterize the internal structure of monomer units. The first peak of $g_{CC}(r)$ (at 1.56 Å) corresponds to the distance between bonded carbon atoms; the second and third peaks (at $r = 2.59$ Å and 2.99 Å, respectively) correspond to the distances between the carbon atoms in the rings. When $r \gtrsim 18$ Å, the PCF is close to 1, thereby demonstrating that there are no long-range correlations in the cross-linked epoxy matrix, i.e., it is amorphous. The number of the cross-links influences the distance between monomers. When the conversion C is increased, the amplitudes of the fourth and fifth peaks of the PCFs, which characterize the intermonomer correlations, increase and the amplitude of the sixth peak decreases. This means that the distance between monomers becomes shorter with increasing the number of cross-links. This can be seen more clearly in Figure 7 where the monomer−monomer PCFs are plotted for the distances between the centers-of-mass of the EP and CA monomers. The positions of the peaks observed for these PCFs shift toward shorter intermonomer distances and their amplitudes increase with C increasing. Therefore, when new cross-links form, the average distance between the EP and CA monomers becomes shorter. In other words, we observe the shrinkage of the system. It is clear that this should lead to an increase in the system density.

Density. In Figure 8 the system density ρ is plotted as a function of C. At small C, the dependence of ρ on C can be approximated by a linear function. However, when the conversion is large enough, $N_{links}/N_{link}^{(max)} \gtrsim 0.5$, the value of ρ approaches a constant. This behavior can be explained by the fact that the minimum volume per monomer is reached when $C \gtrsim 50\%$. For the maximal achievable calculated conversion, we found that $\rho = 1.13 \pm 0.01$ g/cm^3. This value is close to the experimental value of 1.175 ± 0.005 g/cm^3.

In order to analyze the finite size effect, we also simulated the epoxy cross-linking process with different number of the polymerizing monomers (from 8 to 80 EP monomers and from 16 to 160 CA monomers) at the highest achievable conversion and the fixed N_{EP}:N_{CA} ratio ($N_{CA} = 2N_{EP}$). The system density is plotted as a function of N_{EP} in Figure 9. As seen, ρ is weakly dependent on N_{EP}, showing only a very slow increase with the system size increasing. In the case of the largest simulated system ($N_{CA} = 2N_{EP} = 160$), we have: $\rho = 1.14 \pm 0.01$ g/cm^3. The density obtained from the simulation is a little ca. 3% lower than the experimental value. This difference can be due to the force field parameters used in the simulation and to a little lower cross-linking conversion than the realistic one.

Figure 10 shows the simulated density ρ as a function of temperature for different values of C. Each point in this plot represents the average of several consecutive independent runs. The density is found to be a decreasing function of temperature, as expected. It is seen that for the highly cross-linked systems

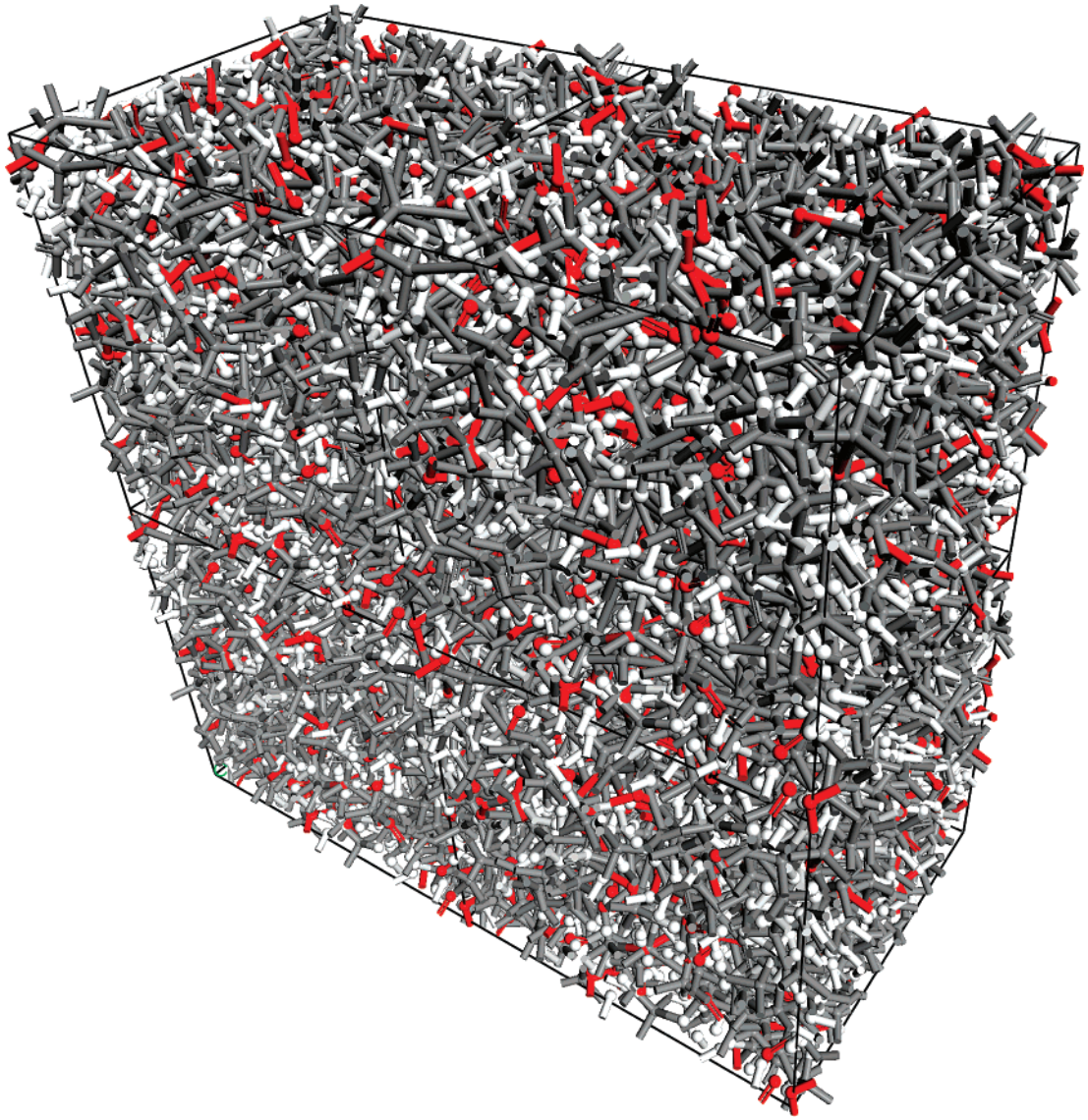

Figure 5. Snapshot picture of a fully atomistic cross-linked polymer system. Atom sizes in this figure are not to scale. The periodic nature of the system is shown as segments leaving one edge of the central unit cell enter on the opposite side.

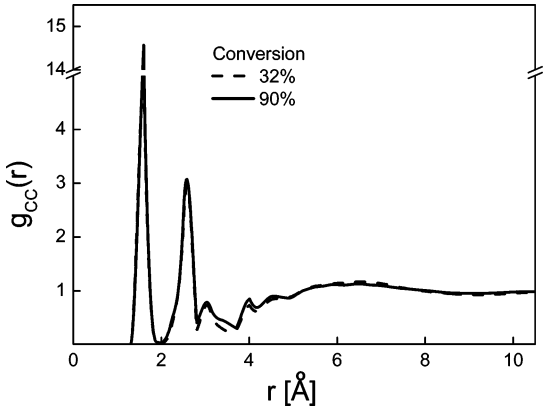

Figure 6. Carbon−carbon pair correlation functions $g_{CC}(r)$ for two cross-linking conversions C, at $N_{EP} = 64$, $N_{CA} = 128$, $T = 298$ K, and $P = 1$ atm. The functions were averaged over 5 independent reverse-mapped atomistic simulations.

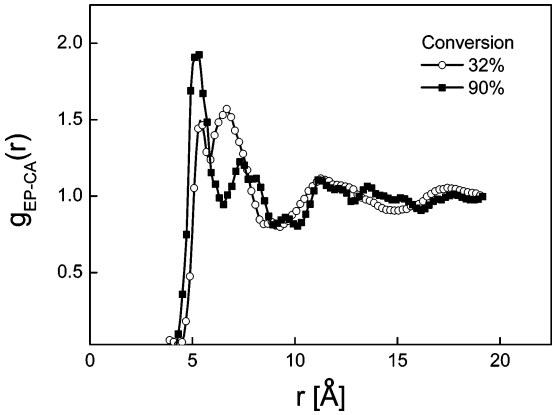

Figure 7. Monomer−monomer pair correlation functions $g_{EP-CA}(r)$ for two cross-linking conversions C, at $N_{EP} = 64$, $N_{CA} = 128$, $T = 298$ K, and $P = 1$ atm. The functions were averaged over 5 independent reverse-mapped atomistic simulations.

($C \gtrsim 45\%$), there are two regions in which the $\rho(T)$ dependence can be approximated by linear functions with different slopes.

Glass Transition Temperature. There are many factors which can affect the glass transition. In the present case, the degree of cross-linking, the network topology and the free volume are three of the main factors. The glass transition temperature, T_g, was determined from the temperature dependence of the system density.[98−104] A plot of ρ vs temperature is shown in Figure 10a. The intercept of the best-fit lines to the simulated data obtained at $C = 90\%$ gave a calculated T_g of

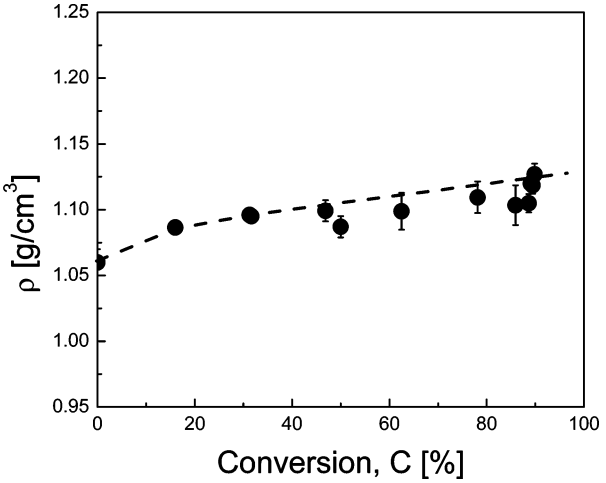

Figure 8. Density of the epoxy system as a function of the cross-linking conversion C for $N_{EP} = 64$ and $N_{CA} = 128$, at $T = 298$ K and $P = 1$ atm. Each data point represents an average over the simulations of 5 sample sets with different initial conditions. The statistical uncertainties are indicated by error bars. Dashed line is provided for eye guidance.

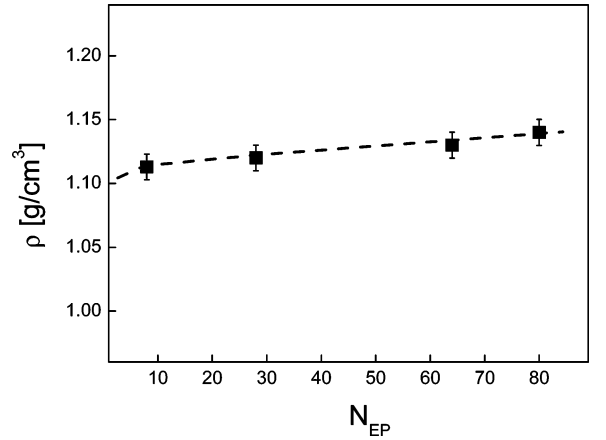

Figure 9. Density of the highly cross-linked epoxy systems as a function of the number of epoxy monomers N_{EP} in the simulation box for $C \approx 93\%$, at $T = 298$ K and $P = 1$ atm. The statistical uncertainties are indicated by error bars. Dashed line is provided for eye guidance.

422 K. The experimental value for this system is 440.5 ± 2.5 K as determined by mechanical thermal analysis (see section 2).

Note that the estimated value of T_g decreases as the effective conversion is reduced (cf. Figure 10b). These results have a clear explanation. It is well-known that the glass transition temperature and many other properties of polymer networks depend on the number of repeat units between cross-link points. If a network is sparse, its glass transition temperature weakly depends on it, but when the number of the repeat units in the chains between neighboring cross-links decreases significantly, the glass transition temperature sharply increases and can reach high values. Our simulations indicate that the glass transition temperature begins to increase when the number of monomer units in linear fragments between cross-links becomes smaller than about 5.

The T_g for the largest sample size case was found to be around 425 K, which is higher than T_g for small sample cases. This is due to the dependence of the T_g on molecular weights of polymer chains formed in the epoxy cross-linking process.

The good agreement of the calculated and experimental values of T_g is indicative of the validity of the simulation. The results indicate that simulated T_gs can be obtained accurately to within

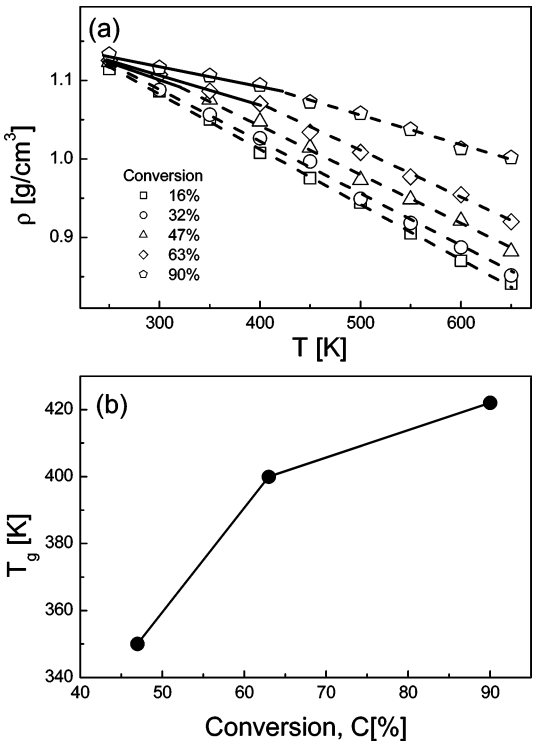

Figure 10. (a) Density as a function of the temperature for different conversion ratios, at $N_{EP} = 64$ and $N_{CA} = 128$. Each data point for a given conversion represents an average over the simulations of five sample sets with different initial conditions. The location of the discontinuity in the slope of the density vs temperature plot indicates the position of the glass transition temperature (T_g). Below T_g, the system is in glassy state, and above T_g, the system will be in a rubberlike or liquid state, if temperature is higher than melting temperature. (b) T_g as a function of the percentage conversion.

≈15−18 K of the actual experimental value, providing confidence in the prediction of the T_g of other epoxy polymers. The level of accuracy found here for a highly cross-linked network system is comparable with that found in the literature simulations of linear polymers.[105]

It should be borne in mind that the simulated values represent the T_g of a "perfect" polymer system and the model does not take into account any defects, areas of crystallinity or voids which might yield a T_g at variance with the simulation results. Nevertheless, accurate results can be achieved with relatively simple models such as this. It would also be possible with this model to perform further simulations around the simulated T_g value in order to determine more accurately the position of the large increase in volume thermal expansion coefficient and hence the position of T_g more precisely. It should be emphasized that the simulated T_g was actually obtained for this epoxy system first and corroborated by the experimental result, making it a true prediction and allowing no bias of the simulation to occur.

Volume Thermal Expansion Coefficient. The decreasing densities of the cross-linked polymer with increasing temperatures indicate the thermal expansion of the material. The slope of the curve at a given temperature gives the volume thermal expansion coefficient $\beta = \rho^{-1}(\partial\rho/\partial T)_{P=\text{const}}$. From the data shown in Figure 10a, the volume thermal expansion coefficient for the glassy state was calculated at room temperature for different C. A plot of β vs C is presented in Figure 11. As in the case of T_g, reasonable agreement with our experimental data was obtained for the maximal achievable calculated conversion for this system (≈90%). The volume thermal expansion coefficient of the system predicted from the simulations is about 30% larger than that experimentally measured in this study. It

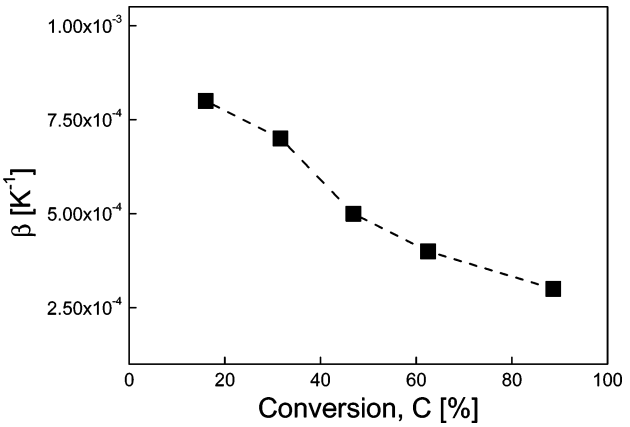

Figure 11. Volume thermal expansion coefficient β for the glassy state as a function of the percentage conversion at room temperature, $T = 298$ K. The dashed line is provided for eye guidance.

is possible that the additional cross-linking of polymer matrix may further reduce the motions of polymer molecules and decrease the β. The MD simulations on smaller sized samples show a larger thermal expansion coefficient, whereas the expansion coefficient in the larger size samples is in better agreement with experimental data.

5. Concluding Remarks

We have developed a computational strategy for simulating the formation of highly cross-linked polymer networks and predicting their structural and thermophysical properties. This methodology based on multiscale simulations involves the following four separate procedures: (i) mapping of the multifunctional polymerizing monomers onto a coarse-grained model, (ii) cross-linking the monomers by applying Monte Carlo (MC) simulation to the coarse-grained model, (iii) reverse mapping of the coarse-grained model to a fully atomistic representation and its further equilibration and refinement, and (iv) simulation of the atomistic model through classical molecular dynamics (MD). Our studies have shown that the atomistic MD itself is very slow to relax a dense highly cross-linked polymer system to its equilibrium conformation. This difficulty is avoided by using intermediate MC simulations. The relaxed systems are then used in subsequent atomistic MD calculations of bulk configurations with periodic boundary conditions.

In order to check the validation of our methodology, we have simulated cycloaliphatic epoxy resins. The same system prepared from 3,4-epoxycyclohexylmethyl-3,4-epoxycyclohexanecarboxylate as resin monomers and 4-methylhexahydrophthalic anhydride as curing agents has been studied experimentally. Using extensive classical MD simulations, we have investigated the thermostructural behavior of the cross-linked epoxy resins. The structural (pair correlation functions) and thermophysical (glass transition temperature and volume thermal expansion coefficient) characteristics of the resins have been studied in the temperature range below and above glass transition temperature T_g, depending on the degree of cross-linking. Good agreement between the computer simulation and experimental results was achieved for highly cross-linked networks, thereby showing that the simulation model is basically valid and the generated polymer network is representative for realistic systems. In particular, we report significant enhancements of the glass transition temperature and volume thermal expansion coefficient of the system as the degree of cross-linking is increased.

Overall, it may be concluded that the results of our simulations are correct and consistent with the experimental data. We may, therefore, expect that it may also be applied successfully to other highly complex networks, including multicomponent systems, used in practice, which are intractable by statistical theories. Our future work will include studying the effects of cross-linking near nanoparticle surfaces and the stress/strain behavior of cross-linked epoxy resins.

Acknowledgment. Financial support from ITRI Elite program, 5C54YAL100, is highly appreciated. P.V.K. also acknowledges the RFBR and the Deutscher Akademischer Austauschdienst (DAAD), German Science Foundation (DFG), for financial support.

References and Notes

(1) Mishnaevsky, L.; Schmauder, S. *Appl. Mech. Rev.* **2001**, *54*, 49.
(2) Schmidt, D. *Curr. Opin. Solid State Mater. Sci.* **2002**, *6*, 205.
(3) Zeng, Q. H.; Yu, A. B.; Lu, G. Q.; Paul, D. R. *J. Nanosci. Nanotechnol.* **2005**, *5*, 1574.
(4) Vacatello, M. *Macromolecules* **2001**, *34*, 1946.
(5) Brown, D.; Mele, P.; Marceau, S.; Alberola, N. D. *Macromolecules* **2003**, *36*, 1395.
(6) Odegard, G. M.; Clancy, T. C.; Gates, T. S. *Polymer* **2005**, *46*, 553.
(7) Qi, D.; Hinkley, J.; He, G. *Model. Simul. Mater. Sci. Eng.* **2005**, *13*, 493.
(8) Barsky, S. J.; Plischke, M. *Phys. Rev. E.* **1996**, *54*, 5370.
(9) Kuhn, W.; Grün, F. *Kolloid-Z.* **1942**, *101*, 248.
(10) Saunders, D. W. *Trans. Faraday Soc.* **1957**, *53*, 860.
(11) Hermans, J. J. *J. Polym. Sci.* **1962**, *58*, 191.
(12) Treloar, L. R. G. *The Physics of Rubber Elasticity*, 3rd ed.; Clarendon Press: Oxford, England, 1975.
(13) Flory, P. J. *J. Chem. Phys.* **1977**, *66*, 5720.
(14) Flory, P. J.; Erman, B. *Macromolecules* **1983**, *16*, 1601; **1983**, *16*, 1607.
(15) Smith, K. J.; Puett, D. *J. Appl. Phys.* **1966**, *37*, 346.
(16) Smith, K. J.; Greene, A.; Ciferri, A. *Kolloid-Z.* **1964**, *194*, 49.
(17) Nagai, K. *J. Chem. Phys.* **1966**, *45*, 838.
(18) Wang, M. C.; Guth, E. *J. Chem. Phys.* **1952**, *20*, 1144.
(19) Smith, K. J.; Ciferri, A.; Hermans, J. J. *J. Polym. Sci., Part A* **1964**, *3*, 1025.
(20) Flory, P. J.; Hoeve, C. A. J.; Cifferri, A. *J. Polym. Sci.* **1959**, *34*, 337.
(21) Mark, J. E.; Erman, B. *Rubberlike Elasticity: A Molecular Primer*; Wiley-Interscience: New York, 1988.
(22) Shibayama, M.; Takata, S.; Norisue, T. *Physica A* **1998**, *249*, 245.
(23) Candau, S.; Bastide, J.; Delsanti, M. *Adv. Polym. Sci.* **1982**, *44*, 27.
(24) Mallam, S.; Horkay, F.; Hecht, A. M.; Geissler, E. *Macromolecules* **1991**, *24*, 543.
(25) Horkay, F.; Hecht, A. M.; Mallam, S.; Geissler, E. *Macromolecules* **1991**, *24*, 2896.
(26) Cohen, Y.; Ramon, O.; Kopelman, I. J.; Mizrahi, S. *J. Polym. Sci., Polym. Phys. Ed.* **1992**, *30*, 1055.
(27) Wu, W.; Shibayama, M.; Roy, S.; Kurokawa, H.; Coyne, L. D.; Nomura, S.; Stein, R. S. *Macromolecules* **1990**, *23*, 2245.
(28) Shibayama, M.; Tanaka, T.; Han, C. C. *J. Chem. Phys.* **1992**, *97*, 6829.
(29) Panyukov, S.; Rabin, Y. *Macromolecules* **1996**, *29*, 7960. Panyukov, S.; Rabin, Y. *Macromolecules* **1996**, *29*, 8530; **1996**, *30*, 301.
(30) Duering, E. R.; Kremer, K.; Grest, G. S. *Phys. Rev. Lett.* **1991**, *67*, 3531.
(31) Grest, G. S.; Kremer, K.; Duering, E. R. *Europhys. Lett.* **1992**, *19*, 195.
(32) Grest, G. S.; Kremer, K.; Duering, E. R. *Physica A* **1993**, *194*, 330.
(33) Duering, E. R.; Kremer, K.; Grest, G. S. *J. Chem. Phys.* **1994**, *101*, 8169−8192.
(34) Depner, M.; Deloche, B.; Sotta, P. *Macromolecules* **1994**, *27*, 5192−5199.
(35) Sommer, J.-U. *Macromol. Symp.* **1994**, *81*, 139−152.
(36) Baljon, A. R. C.; Grest, G. S.; Witten, T. A. *Macromolecules* **1995**, *28*, 1835−1840.
(37) Sotta, P.; Higgs, P. G.; Depner, M.; Deloche, B. *Macromolecules* **1995**, *28*, 7208−7214.
(38) Gao, J.; Weiner, J. H. *J. Chem. Phys.* **1995**, *103*, 1614.
(39) Trautenberg, H.; Sommer, J.-U.; Göritz, D. *J. Chem. Soc., Faraday Trans.* **1995**, *91*, 2649.
(40) Escobedo, F. A.; de Pablo, J. J. *J. Chem. Phys.* **1996**, *104*, 4788−4801.
(41) Hölzl, T.; Trautenberg, H. L.; Göritz, D. *Phys. Rev. Lett.* **1997**, *79*, 2293−2296.
(42) Escobedo, F. A.; de Pablo, J. J. *J. Chem. Phys.* **1997**, *106*, 793−810.
(43) Escobedo, F. A.; de Pablo, J. J. *Mol. Phys.* **1997**, *90*, 437−443.
(44) Sotta, P. *Macromolecules* **1998**, *31*, 8417−8422.

(45) Kenkare, N. R.; Smith, S. W.; Hall, C. K.; Khan, S. A. *Macromolecules* **1998**, *31*, 5861.
(46) Yong, C. W.; Higgs, P. G. *Macromolecules* **1999**, *32*, 5062−5071.
(47) Kenkare, N. R.; Hall, C. K.; Khan, S. A. *J. Chem. Phys.* **1999**, *110*, 7556−7573.
(48) Grest, G. S.; Pütz, M.; Everaers, R.; Kremer, K. *J. Non-Cryst. Solids* **2000**, *274*, 139.
(49) Gilra, N.; Cohen, C.; Panagiotopoulos, A. Z. *J. Chem. Phys.* **2000**, *112*, 6910−6916.
(50) Gilra, N.; Panagiotopoulos, A. Z.; Cohen, C. *Macromolecules* **2001**, *34*, 6090−6096.
(51) Haslam, A. J.; Jackson, G.; McLeish, T. C. B. *Macromolecules* **1999**, *32*, 7289−7298.
(52) Cail, J. I.; Taylor, D. J. R.; Stepto, R. F. T.; Brereton, M. G.; Jones, R. A.; Ries, M. E.; Ward, I. M. *Macromolecules* **2000**, *33*, 4966−4971.
(53) Rankin, S. E.; Kasehagen, L. J.; McCormick, A. V.; Macosko, C. W. *Macromolecules* **2000**, *33*, 7639−7648.
(54) Kindt, J. T. *J. Phys. Chem. B* **2002**, *106*, 8223−8232.
(55) Chen, Z.; Cohen, C.; Escobedo, F. A. *Macromolecules* **2002**, *35*, 3296−3305.
(56) Hutchison, J. B.; Anseth, K. S. *J. Phys. Chem. B* **2004**, *108*, 11097−11104.
(57) Li, H.; Ng, T. Y.; Yew, Y. K.; Lam, K. Y. *Biomacromolecules* **2005**, *6*, 109−120.
(58) Lu, W.; Ding, J. *Macromolecules* **2006**, *39*, 7433−7440.
(59) Chiessi, E.; Cavalieri, F.; Paradossi, G. *J. Phys. Chem. B* **2007**; ASAP Article.
(60) Hamerton, I.; Heald, C. R.; Howlin, B. J. *J. Mater. Chem.* **1996**, *6*, 311−314.
(61) Hamerton, I.; Howlin, B. J.; Klewpatinond, P.; Takeda, S. *Polymer* **2002**, *43*, 4599−604.
(62) Hamerton, I.; Howlin, B. J.; Klewpatinond, P.; Shortley, H. J.; Takeda, S. *Polymer* **2006**, *47*, 690.
(63) Doherty, D. C.; Holmes, B. N.; Leung, P.; Ross, R. B. *Comput. Theor. Polym. Sci.* **1998**, *8*, 169.
(64) Yarovsky, I.; Evans, E. *Mol. Simul.* **2002**, *28*, 993−1004.
(65) Heine, D. R.; Grest, G. S.; Lorenz, C. D.; Tsige, M.; Stevens, M. J. *Macromolecules* **2004**, *37*, 3857.
(66) Lee, H.; Neville, K. *Handbook of Epoxy Resins*; McGraw-Hill: New York, 1967.
(67) Goodman, S. H. *Handbook of Thermoset Plastics*; Noyes: Boston, MA, 1986; pp 133−182.
(68) Brydson, J. A. *Plastics Materials*; Iliffe Books Ltd./D. Van Nostrand Co.: London, 1966; pp 451−483.
(69) Alperstein, D.; Dodiuk, H.; Kenig, S. *Acta Polym.* **1998**, *49*, 594−599.
(70) *"Polymer" Manual*; MSI: San Diego, CA, 1995.
(71) Wu, C.; Xu, W. *Polymer* **2006**, *47*, 6004−6009.
(72) Accelrys Inc., San Diego, CA.
(73) Yarovsky, I.; Evans, E. *Polymer* **2002**, *43*, 963.
(74) Baschnagel, J.; Binder, K.; Doruker, P.; Gusev, A. A.; Hahn, O.; Kremer, K.; Mattice, W. L.; Müller-Plathe, F.; Murat, M.; Paul, W.; Santos, S.; Suter, W. W.; Tries, V. *Adv. Polym. Sci.* **2000**, *152*, 41−155.
(75) Doruker, P.; Mattice, W. L. *Macromolecules* **1997**, *30*, 5520.
(76) Doruker, P.; Mattice, W. L. *Macromol. Theory Simul.* **1999**, *8*, 463.
(77) Kremer, K.; Müller-Plathe, F. *Mater. Res. Soc. Bull.* **2001** (March), 205−214.
(78) Müller-Plathe, F. *Chem. Phys. Chem.* **2002**, *3*, 754−769.
(79) Kremer, K.; Müller-Plathe, F. *Mol. Simul.* **2002**, *28*, 729−750.
(80) Glotzer, S. C.; Paul, W. *Annu. Rev. Mater. Res.* **2002**, *32*, 401−436.
(81) Müller-Plathe, F. *Soft Mater.* **2003**, *1*, 1.
(82) Clancy, T. C. *Polymer* **2004**, *45*, 7001.
(83) Santangelo, G.; Di Matteo, A.; Müller-Plathe, F.; Milano, G. *J. Phys. Chem. B* **2007**, *111*, 2765.
(84) May, C. A. *Epoxy Resins*; Marcel Dekker: New York, 1988.
(85) Weber, T. A.; Helfand, E. *J. Chem. Phys.* **1979**, *71*, 4760.
(86) *Cycloaliphatic Epoxide Systems*; Union Carbide Corp.: Bound Brook, NJ, 1989.
(87) Metropolis, N.; Rosenbluth, A. W.; Rosenbluth, M. N.; Teller, A. N.; Teller, E. *J. Chem. Phys.* **1953**, *21*, 1087.
(88) Jorgensen, W. L.; Madura, J. D.; Swenson, C. J. *J. Am. Chem. Soc.* **1984**, *106*, 6638−6646.
(89) Jorgensen, W. L. *J. Phys. Chem.* **1986**, *90*, 1276−1284.
(90) Jorgensen, W. L.; McDonald, N. A. *THEOCHEM J. Mol. Struct.* **1998**, *424*, 145.
(91) McDonald, N. A.; Jorgensen, W. L. *J. Phys. Chem. B* **1998**, *102*, 8049.
(92) Plimpton, S. J.; Pollock, R.; Stevens, M. Particle-Mesh Ewald and rRESPA for Parallel Molecular Dynamics Simulation. *Proceedings of the Eighth SIAM Conference on Parallel Processing for Scientific Computing*, March, 1997, Minneapolis, MN.
(93) Nose, S. *Mol. Phys.* **1986**, *57*, 187. Hoover, W. G. *Phys. Rev. A* **1985**, *31*, 1695.
(94) Martyna, G. J.; Tobais, D. J.; Klein, M. L. *J. Chem. Phys.* **1994**, *101*, 4177.
(95) Tuckerman, M.; Berne, B. J.; Martyna, G. J. *J. Chem. Phys.* **1992**, *97*, 1990.
(96) Allen, M. P.; Tildesley, D. J. *Computer Simulation of Liquids*; Claredon: Oxford, 1987.
(97) Verlet, L. *Phys. Rev.* **1967**, *159*, 98.
(98) Roe, R. J. *Computer Simulation of Polymer*; Prentice−Hall, Englewood, Cliffs, NJ, 1991.
(99) Rigby, D.; Roe, R. J. *J. Chem. Phys.* **1987**, *87*, 7285. Rigby, D.; Roe, R. J. *J. Chem. Phys.* **1988**, *89*, 5280. Rigby, D.; Roe, R. J. *Macromolecules* **1989**, *22*, 2259.
(100) Boyd, R. H.; Pant, P. V. K. *Macromolecules* **1991**, *24*, 4078.
(101) Mansfield, K. F.; Theodorou, D. N. *Macromolecules* **1991**, *24*, 6283.
(102) Ekdawi-Sever, N. C.; Conrad, P. B.; de Pablo, J. J. *J. Phys. Chem. A* **2001**, *105*, 734.
(103) Pozuelo, J.; Baselga, J. *Polymer* **2002**, *43*, 6049.
(104) Morita, H.; Tanaka, K.; Kajiyama, T.; Nishi, T.; Doi, M. *Macromolecules* **2006**, *39*, 6233.
(105) Binder, K.; Baschnagel, J.; Paul, W. *Prog. Polym. Sci.* **2003**, *28*, 115−172.

MA070702+